42nd AIAA Thermophysics Conference
27 - 30 June 2011, Honolulu, Hawaii

AIAA 2011-3310

Computational Analysis of Rarefied Hypersonic Flow over a Forward-Facing Step

Paulo H. M. Leite* and Wilson F. N. Santos†

National Institute for Space Research, Cachoeira Paulista, SP, 12630-000, BRAZIL

The present work performs a computational study on rarefied hypersonic flow past a forward-facing step at zero-degree angle of attack in chemical equilibrium and thermal non-equilibrium. Effects on the aerodynamic surface quantities due to changes on the frontal-face height of the step have been investigated by employing the Direct Simulation Monte Carlo (DSMC) method. The work focuses the attention of designers of hypersonic configurations on the fundamental parameter of surface discontinuity, which can have an important impact on even initial design. The results presented highlight the behavior of the heat transfer, pressure, and skin friction coefficients to changes on the frontal-face height. The analysis showed that hypersonic flow past a forward-facing step is characterized by a strong compression ahead of the frontal face, which influences the aerodynamics surface properties upstream the frontal face. Locally high heating and pressure loads were observed on three locations along the surface, i.e., on the lower surface, on the frontal face and on the upper surface. Results showed that both loads rely on the frontal-face height. The peak values for the heat transfer coefficient on the frontal face surface were at least one order of magnitude larger than the maximum value observed for a smooth surface, i.e., a flat plate without a step.

Nomenclature

a	Speed of sound, m/s
C_f	Skin friction coefficient, Eq.(5)
C_h	Heat transfer coefficient, Eq.(1)
C_p	Pressure coefficient, Eq.(3)
c	Molecular velocity, m/s
d	Molecular diameter, m
D	Total length, m
h	Frontal-face height, m
H	Dimensionless frontal-face height, h/λ_∞
Kn	Knudsen number, λ/h
L	Upstream surface length, m
M	Mach number, U/a
m	Molecular mass, kg
n	Number density, m^{-3}
N	Number of molecules
N_f	Dimensionless number flux, $N/n_\infty U_\infty$
p	Pressure, $\mathrm{N/m}^2$
q	Heat flux, $\mathrm{W/m}^2$
Re	Reynolds number, Uh/μ
R	Reentry capsule nose radius, m
T	Temperature, K
u, v	Normal and tangential velocity components, m/s

*Graduate Student, Combustion and Propulsion Laboratory.
†Researcher, Combustion and Propulsion Laboratory, and AIAA Member.

U Freestream velocity, m/s
x, y Cartesian axes in physical space, m
X Dimensionless length, x/λ_∞
Y Dimensionless height, y/λ_∞
α Angle of attack, degree
λ Molecular mean free path, m
μ Viscosity, Ns/m^2
ρ Density, kg/m^3
τ Shear stress, N/m^2
ω Viscosity index, dimensionless

Subscript
w Refers to wall conditions
∞ Refers to freestream conditions

I. Introduction

In the design of a hypersonic vehicle, the knowledge of the factors that affect the thermal and aerodynamic loads acting on the vehicle surface becomes imperative. Usually, in the calculations of the thermal and aerodynamic loads, the analysis assumes that the vehicle has a smooth surface. However, discontinuities, such as steps, cavities and gaps, are often present on the vehicle surface due to, for instance, fabrication tolerances, sensor installations, and differential expansion or ablation rates between non-similar materials (Bertram and Wiggs,[1] Hahn,[2] Nestler et al.,[3] and Grotowsky and Ballmann[4]). Such surface discontinuities may constitute in a potential source in a heat flux rise to the surface or even though in a premature transition from laminar to turbulent flow.

In hypersonic flight, the flow over a step, cavity or gap causes locally thermal and aerodynamic loads that may dramatically exceed those ones of a smooth contour. In order to operate safely, these loads have to be predicted correctly. This can be done either by experiments, which are often very expensive for real flight conditions, or by numerical simulation, which is getting continuously increasing importance.

For the particular case of a forward-facing step, many experimental and theoretical studies (Nestler et al.,[3] Grotowsky and Ballmann,[4] Chapmann et al.,[5] Rogers and Berry,[6] Pullin and Harvey,[7] Stuer et al.,[8] Camussi et al.,[9] and Bogdonoff and Kepler[10]) have been conducted in order to understand the physical aspects of a subsonic, supersonic or hypersonic flow past to this type of discontinuity, characterized by a sudden change on the surface slope. For the purpose of this introduction, it will be sufficient to describe only a few of these studies.

Nestler et al.[3] conducted an experimental investigation on steps and cavities in a hypersonic turbulent flow. For the flow conditions investigated, they found that the pressure distributions in the cavity presented a typical behavior of closed cavity flow in the sense that the flow expands into the cavity, reattaches to the floor, and separates as it approaches the downstream corner.

Grotowsky and Ballmann[4] investigated laminar hypersonic flow over forward- and backward-facing steps by employing Navier-Stokes equations. The hypersonic flow over the steps were simulated by considering freestream Mach number of 8, Reynolds number of the order of 10^8 and an altitude of 30 km. According to them, the computational results presented a good agreement with the experimental data available in the literature. They also pointed out that the quantitative comparison exhibited major differences for the wall heat flux, probably due to the difficult in how to measure accurately.

Pullin and Harvey[7] numerically analyzed a two-dimensional rarefied hypersonic flow around a forward-facing step by considering N_2 as the working fluid and freestream Mach number of 22. The analysis showed that, at the vicinity of the step base, the flow has a rapid deceleration and compression accompanied by a sudden transition to a near continuum Navier-Stockes-type state nearly in equilibrium at the step temperature. In addition, their computational results presented good agreement with experimental data.

Bogdonoff and Kepler[10] conducted a experimental investigation on separation associated with steps and shock-wave boundary-layer interaction in the continuum flow regime. For freestream Mach number around 3, the experiments showed that separation occurred at a pressure ratio of about 2 for the forward-facing steps investigated. In addition, combined with other investigations, the results indicated a very small variation of the separation pressure ratio with Mach number.

According to the current literature, there have been considerable experimental and theoretical studies

conducted to understand the physical aspects of a subsonic, supersonic or hypersonic flow past to steps. The major interest in these studies has gone into considering laminar or turbulent flow in the continuum flow regime. However, there is little understanding of the physical aspects of hypersonic flow past to steps related to the severe aerothermodynamic environment associated with a reentry vehicle. In this scenario, the purpose of the present account is to investigate the flowfield structure of a hypersonic flow on a forward-facing step in the transition flow regime, i.e., between the continuum flow and the free collision flow regime. The focus of the present study is the low-density region in the upper atmosphere, where numerical gaskinetic procedures are available to simulate hypersonic flows. High-speed flows under low-density conditions deviate from a perfect gas behavior because of the excitation of rotational and vibrational modes. At high altitudes, and therefore, low density, the molecular collision rate is low and the energy exchange occurs under non-equilibrium conditions. In such a circumstance, the degree of molecular non-equilibrium is such that the Navier-Stokes equations are inappropriate. Consequently, the Direct Simulation Monte Carlo (DSMC) method will be employed to calculate the hypersonic two-dimensional flow on the forward-facing step.

II. Geometry Definition

In the present account, discontinuities or imperfections present on the surface of a reentry capsule is modeled by a forward-facing step. By considering that the step frontal-face h is much smaller than the nose radius R of a reentry capsule, i.e., $h/R \ll 1$, then the hypersonic flow over the step may be considered as a hypersonic flow over a flat plate with a forward-facing step. Figure 1 displays a schematic view of the model employed and presents the important parameters.

According to Fig. 1, M_∞ represents the freestream Mach number, α refers to the angle of attack, h the frontal-face height, L the length of the step upstream surface, and D the total length of the flat plate. It was considered that the flat plate is infinitely long but only the total length D is examined. It was assumed a frontal-face height h of 3, 6, and 9 mm, which correspond to $H(= h/\lambda_\infty)$ of 3.23, 6.46, and 9.69, respectively, where λ_∞ is the freestream mean free path. In addition, it was assumed L/λ_∞ of 50 and D/λ_∞ of 100.

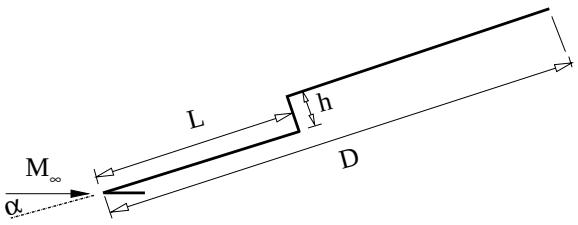

Figure 1. Drawing illustrating the forward-facing step.

An understanding of the frontal-face height impact on the flowfield structure can be gained by comparing the flowfield behavior of a flat plate with a step to that of a flat plate without a step. In this fashion, a flat plate free of discontinuities, i.e, without steps, works as a benchmark for the cases with steps.

III. Computational Method and Procedure

Flows are characterized by a variety of dimensionless quantities. The most useful one for the purpose of this work is the Knudsen number Kn. The degree of rarefaction of a flow is usually expressed through the overall Knudsen number, $Kn = \lambda/l$, where λ is the mean free path in the freestream gas and l is a characteristic length of the flowfield. The conventional continuum flow assumption is valid when the overall Knudsen number tends to zero. In this flow regime, one can disregard its microscopic structure and consider only its macroscopic properties such as density, velocity, pressure, or temperature. In the opposite limit, the overall Knudsen number tending to infinity, the flow regime corresponds to the free molecular flow. In this case, intermolecular collisions may be neglected and particle collisions with the body surface play the determining role. The region defined by $0.1 < Kn < 10$ is referred to as the transitional flow regime, where not only gas-surface collisions but also intermolecular collisions are important.

It is well known that neither the continuum flow equations nor the collisionless flow equations are valid to predict the flowfield characteristics throughout the transitional flow regime. During the last several years, the most successful numerical technique applied for computing flowfield structure in the transition flow regime has been the Direct Simulation Monte Carlo (DSMC) method pioneered by Bird.[11] The DSMC method simulates real gas flows with various physical processes by means of a huge number of modeling particles,

each of which is a typical representative of a great number of real gas molecules. DSMC models the flow as being a collection of discrete particles, each one with a position, velocity and internal energy. The state of particles is stored and modified with time as the particles move, collide, and undergo boundary interactions in simulated physical space.

In the present account, the molecular collision kinetics are modeled by using the variable hard sphere (VHS) molecular model,[12] and the no time counter (NTC) collision sampling technique.[13] Energy exchange between kinetic and internal modes is controlled by the Borgnakke-Larsen statistical model.[14] Simulations are performed using a non-reacting gas model, consisting of 76.3% of N_2 and 23.7% of O_2, while considering energy exchange between translational, rotational and vibrational modes. For a given collision, the probability is defined by the inverse of the number of relaxation, which corresponds to the number of collisions needed, on average, for a molecule undergoes relaxation. The probability of an inelastic collision determines the rate at which energy is transferred between the translational and internal modes after an inelastic collision. Relaxation collision numbers of 5 and 50 were used for the calculations of rotation and vibration, respectively.

IV. Computational Flow Domain and Grid

For the numerical treatment of the problem, the flowfield around the forward-facing step is divided into an arbitrary number of regions, which are subdivided into computational cells. The cells are further subdivided into subcells, two subcells/cell in each coordinate direction. The cell provides a convenient reference for the sampling of the macroscopic gas properties, while the collision partners are selected from the same subcell for the establishment of the collision rate.

The computational domain used for the calculation is made large enough so that body disturbances do not reach the upstream and side boundaries, where freestream conditions are specified. A schematic view of the computational domain is depicted in Fig. 2. According to this figure, side I-A is defined by the forward-facing step surface. Diffuse reflection with complete thermal accommodation is the condition applied to this side. In a diffuse reflection, the molecules are reflected equally in all directions, and the final velocity of the molecules is randomly assigned according to a half-range Maxwellian distribution determined by the wall temperature. Side I-B is a plane of symmetry, where all flow gradients normal to the plane are zero. At the molecular level, this plane is equivalent to a specular reflecting boundary. Sides II and III are the freestream sides through which simulated molecules enter and exit. Side II is positioned at $5\lambda_\infty$ upstream of the flat-plate leading edge, and side III defined at $30\lambda_\infty$, $34\lambda_\infty$, and $42\lambda_\infty$ above the step upper surface for frontal-face height H of 3.23, 6.46, and 9.69, respectively. Finally, the flow at the downstream outflow boundary, side IV, is predominantly supersonic and vacuum condition is specified.[15] At this boundary, simulated molecules can only exit.

DSMC results depend on the cell size chosen, on the time step as well as on the number of particles per computational cell. In the DSMC code, the linear dimensions of the cells should be small in comparison with the length scale of the macroscopic flow gradients normal to the streamwise directions, which means that the cell dimensions should be the order of or smaller than the local mean free path.[16,17] The time step should be chosen to be sufficiently small in comparison with the local mean collision time.[18,19] A very small time step results in an inefficient advancement of the solution and accumulation of statistics. Most particles will take many time steps to cross a given cell. As a result, the collision phase of each time step will involve the same group of particles as in the previous time step since almost no particles leave or enter the cell. Moreover, a large time step allows the molecules to move too far without the opportunity to participate in a collision. This again causes a smearing

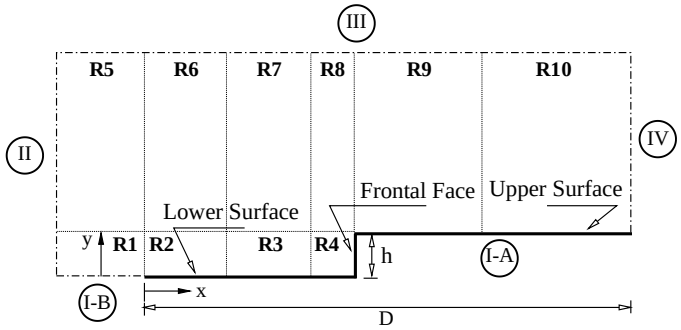

Figure 2. Drawing illustrating the computational domain.

Table 1. Number of cells in the (x-direction) and [y-direction] for the $H = 3.23$ case.

	Coarse	Standard	Fine
Region 1	$(5 \times 10)[10 \times 5]$	10×10	$(20 \times 10)[10 \times 20]$
Region 2	$(20 \times 30)[40 \times 15]$	40×30	$(80 \times 30)[40 \times 60]$
Region 3	$(20 \times 30)[40 \times 15]$	40×30	$(80 \times 30)[40 \times 60]$
Region 4	$(30 \times 70)[60 \times 35]$	60×70	$(120 \times 70)[60 \times 140]$
Region 5	$(5 \times 40)[10 \times 20]$	10×40	$(20 \times 40)[10 \times 80]$
Region 6	$(15 \times 40)[30 \times 20]$	30×40	$(60 \times 40)[30 \times 80]$
Region 7	$(15 \times 40)[30 \times 20]$	30×40	$(60 \times 40)[30 \times 80]$
Region 8	$(15 \times 50)[30 \times 25]$	30×50	$(60 \times 50)[30 \times 100]$
Region 9	$(30 \times 70)[60 \times 35]$	60×70	$(120 \times 70)[60 \times 140]$
Region 10	$(30 \times 80)[60 \times 40]$	60×80	$(120 \times 80)[60 \times 160]$

of the properties of the flow, resulting in non-physical results; therefore, the time step must be chosen such that a typical particle moves about one fourth of the cell dimension at each time step. Finally, the number of simulated particles has to be large enough to make statistical correlations between particles insignificant.

A grid independence study was made with three different structured meshes – coarse, standard and fine – in each coordinate direction. The effect of altering the cell size in the x- and y-directions was investigated for a coarse and fine grids with, respectively, 50% less and 100% more cells with respect to the standard grid. In addition, each grid was made up of non-uniform cell spacing in both directions. Moreover, point clustering was used close to solid walls. Table 1 tabulates the number of cells employed in the ten regions (R1 to R10 in Fig. 2) for coarse, standard, and fine grids for the $H = 3.23$ case. The effect (not shown) of changing the cell size in both directions on the heat transfer, pressure and the skin friction coefficients was rather insensitive to the range of the cell spacing considered, indicating that the standard grid, with a total of 20,000 cells for the $H = 3.23$ case, is essentially grid independent.

In a second stage of the grid independence investigation, a similar examination was made for the number of molecules. The standard grid for the $H = 3.23$ case corresponds to, on average, a total of 420,000 molecules. Two new cases using the same grid were investigated. These two new cases corresponded to 210,000 and 840,000 molecules in the entire computational domain. As the three cases presented the same results (not shown) for the heat transfer, pressure and skin friction coefficients, hence the standard grid with a total of 420,000 molecules was considered enough for the computation of the aerodynamic surface quantities.

A similar procedure for the grid independence study was performed for the other two cases. As a result, for H of 6.46 and 9.69, the standard grid corresponded, respectively, to the total of 33,800 and 41,600 cells, with a total of 710,400 and 896,300 molecules. A discussion of the verification process, effects of the cell size, time step, and number of molecules on the aerodynamic surface quantities for the forward-facing steps presented herein, is described in detail by Leite.[20]

V. Freestream and Flow Conditions

Freestream conditions employed in the present calculations are those given by Leite[20] and tabulated in Tab. 2. These flow conditions represent those experienced by a Brazilian capsule, named SARA (acronyms for SAtélite de Reentrada Atmosférica) at an altitude of 70 km. In addition, the gas properties[11] considered

Table 2. Freestream flow conditions

Altitude (km)	T_∞(K)	p_∞(N/m^2)	ρ_∞(kg/m^3)	μ_∞(Ns/m^2)	n_∞(m^{-3})	λ_∞(m)
70	220.0	5.582	8.753×10^{-5}	1.455×10^{-5}	1.8209×10^{21}	9.03×10^{-4}

in the simulation are listed in Tab. 3. Referring to Tabs. 2 and 3, T_∞, p_∞, ρ_∞, μ_∞, n_∞, λ_∞, and U_∞ stand respectively for temperature, pressure, density, viscosity, number density, and mean free path, and X, m, d, and ω account respectively for mole fraction, molecular mass, molecular diameter and viscosity index.

The freestream velocity U_∞ is assumed to be constant at 7456 m/s, which corresponds to a freestream Mach number M_∞ of 25. The wall temperature T_w is assumed constant at 880 K. This temperature is chosen to be representative of the surface temperature near the stagnation point of a reentry capsule and is assumed to be uniform over the forward-facing step. It is important to mention that the surface temperature is low compared to the stagnation temperature of the air. This assumption seems reasonable since practical surface material will probably be destroyed if surface temperature is allowed to approach the stagnation temperature.

Table 3. Gas properties

	X	m (kg)	d (m)	ω
O_2	0.237	5.312×10^{-26}	4.01×10^{-10}	0.77
N_2	0.763	4.650×10^{-26}	4.11×10^{-10}	0.74

By assuming the frontal-face height h as the characteristic length, the Knudsen number Kn_h corresponds to 0.3095, 0.1548 and 0.1032 for height h of 3, 6 and 9 mm, respectively. The Reynolds number Re_h is around 136, 272 and 409 for height h of 3, 6 and 9 mm, respectively, also based on the frontal-face height h and on conditions in the undisturbed stream. Finally, it was assumed zero-degree angle of attack, i.e., $\alpha = 0$.

VI. Computational Results and Discussion

The purpose of this section is to discuss and to compare differences in the aerodynamic surface properties due to variations on the frontal-face height of a forward-facing step. The aerodynamic properties of particular interest in this work are number flux, heat transfer, pressure and the skin friction coefficients.

A. Number Flux

The number flux N is calculated by sampling the molecules impinging on the surface by unit time and unit area. The distribution of the number flux along the step surface – lower, face and upper – is illustrated in Fig. 3 as a function of the dimensionless frontal-face height H. In this group of plots, N_f represents the number flux N normalized by $n_\infty U_\infty$, where n_∞ is the freestream number density and U_∞ is the freestream velocity. In addition, X and Y are the lengths x and y normalized by the freestream mean free path λ_∞. As a basis of comparison, the dimensionless number flux for the flat-plate case, i.e., a flat plate without a step, is also illustrated in the plots.

Looking first to Fig. 3(a), it is observed that the number flux to the surface depends on the frontal-face height H. Close to the sharp leading edge, the behavior of the number flux to the flat plate with a step is similar to that for a flat plate without a step. This is an expected behavior since the flow in this region is not affected by the presence of the step. As the flow develops downstream along the lower surface, the presence of the step is felt in the number flux distribution at section X corresponding to approximately 32.6, 38.1 and 43.4, for frontal-face height H of 9.69, 6.46, and 3.23, respectively. From these sections up to the section where the steps are located, $X = 50$, the number flux to the surface dramatically increases in comparison to the number flux observed for the flat-plate case. This region, where a number flux rise is observed, is directly related to the recirculation zone that forms ahead of the frontal-face of the step. The recirculation zone concentrates a large number of molecules. The molecules enclosed in this region, when colliding with the lower surface and with the face of the step, increase not only the number flux to the lower surface and to the frontal face but also increase the energy exchange as well as the linear momentum.

Turning next to Fig. 3(b), it can be seen that the number flux to the frontal-face surface is more intense than that observed to the lower surface. Similarly to that for the lower surface, the number flux to the frontal face is a function of the step height H, i.e, it increases with the frontal-face height rise. It may be recognized from this figure that the number flux distribution presents two peak values for each case investigated; one of them close to the step base, and the other one at the vicinity of the step corner. It should be remarked that the second peak value takes place at section Y equal to 2.83, 6.09, and 9.21 for H of 3.23, 6.46, and 9.69, respectively. As a matter of fact, the flow reattachment point, Y_r, on the frontal face occurs for section Y equal to 2.69, 5.66 and 8.72 for H of 3.23, 6.46, and 9.69, respectively. It is important to mention that, in

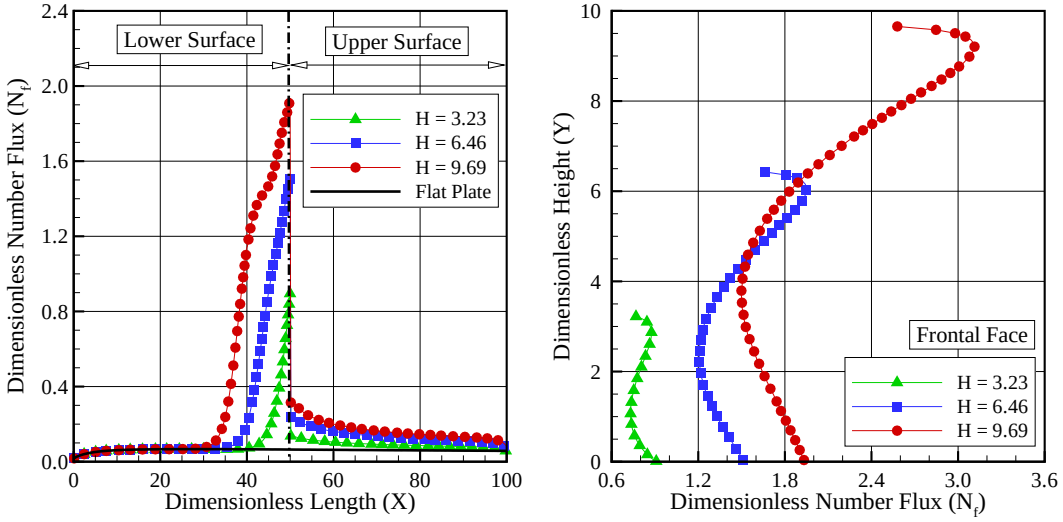

(a) Lower and upper surfaces

(b) Frontal-face surface

Figure 3. Distribution of the number flux N_f along (a) the lower and upper surfaces and along the (b) frontal-face surface as function of the dimensionless frontal-face height H.

the present account, the flow reattachment point on the frontal-face of the step was obtained by assuming the section where the skin friction coefficient C_f changes from negative value to positive one, i.e., $C_f = 0$.

In order to emphasize the recirculation zone and the flow reattachment zone, Figs. 4(a-c) display the streamline traces at the vicinity of the steps. In this set of figures, Y_h stands for the vertical distance y normalized by h, and X_h refers to the horizontal distance $(x - L)$ also normalized by h. In this context, the reference frame was moved to the step position. Taking a closer look at these figures, it is clearly seen that the recirculation zone and the flow reattachment point are a function of the frontal-face height h.

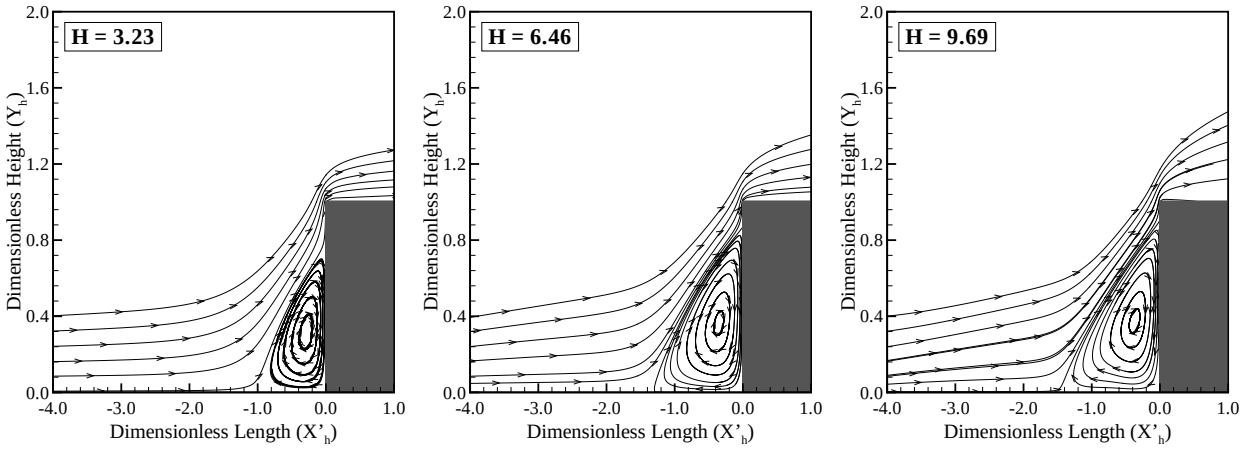

(a) (b) (c)

Figure 4. Streamline traces at the vicinity of the forward-facing step for dimensionless frontal-face height H of (a) 3.23, (b) 6.46, and (c) 9.693.

B. Heat Transfer coefficient

The heat transfer coefficient C_h is defined as follows,

$$C_h = \frac{q_w}{\frac{1}{2}\rho_\infty U_\infty^3} \tag{1}$$

where the heat flux q_w to the body surface is calculated by the net energy flux of the molecules impinging on the surface. A flux is regarded as positive if it is directed toward the body surface. The net heat flux q_w is related to the sum of the translational, rotational and vibrational energies of both incident and reflected molecules as defined by,

$$q_w = q_i - q_r = \frac{F_N}{A\Delta t}\{\sum_{j=1}^{N}[\frac{1}{2}m_j c_j^2 + e_{Rj} + e_{Vj}]_i - \sum_{j=1}^{N}[\frac{1}{2}m_j c_j^2 + e_{Rj} + e_{Vj}]_r\} \tag{2}$$

where F_N is the number of real molecules represented by a single simulated molecule, Δt is the time step, A the area, N is the number of molecules colliding with the surface by unit time and unit area, m is the mass of the molecules, c is the velocity of the molecules, e_R and e_V stand for rotational and vibrational energies, respectively. Subscripts i and r refer to incident and reflect molecules.

The dependence of the heat transfer coefficient C_h on the frontal-face height h is demonstrated in Figs. 5(a,b) for the lower, frontal face, and upper surfaces. According to this set of figures, important features can be observed in the heat transfer coefficient behavior. Of particular interest, it is observed that: (1) similar to the number flux, the heat transfer coefficient C_h for forward-facing steps follows the same behavior presented by the flat-plate case close to the sharp leading edge, region unaffected by the presence of the steps, (2) further downstream along the lower surface, the heat transfer coefficient C_h significantly increases and reaches peak values close to the frontal face, then decreases to almost zero at the stagnation region, (3) along the upper surface, the heat transfer coefficient presents a maximum value at the step corner and then decreases downstream along the surface, almost reaching the values observed for the flat-plate case, (4) along the frontal face, the heat transfer coefficient increases monotonically, from zero at the stagnation point to a maximum value near the step corner, which depends on the frontal-face height h, (5) it is quite apparent that this significant increase in the heat transfer coefficient is due to the flow reattachment zone, finally, (6) the maximum values observed for the heat transfer coefficient on the frontal-face surface is an order of magnitude greater than those observed on the lower surface. For comparative purpose, the maximum values for C_h are around 0.22, 0.38 and 0.52 for height H of 3.23, 6,46 and 9.69, respectively. In contrast, the C_h for the flat-plate case, i.e., a flat plate without steps, is around 0.0284 at section $X = 9.11$ in the lower surface. Therefore, C_h of 0.22, 0.38 and 0.52 correspond respectively to 7.75, 13.38 and 18.31 times the pick value for the flat-plate case. Furthermore, it is very encouraging to observe that, for the $H = 9.69$ case, the amount of energy transferred to the step corner represents around 50% of the total energy ($\rho_\infty U_\infty^3/2$) of the gas coming from the freestream.

Another feature of particular interest in the heat transfer coefficient behavior is related to the peak values on the lower surface due to the presence of the step. As shown in Fig. 5(a), the maximum values observed for the heat transfer coefficient C_h as well as the location in which they occur depend on the frontal-face height H. For height H of 3.23, 6.46, and 9.69, the maximum values for the heat transfer coefficient C_h correspond to section X of 47.5, 42.4, and 37.0, respectively. Nevertheless, the separation point corresponds to section X_s of 48.3, 42.8, and 37.2 for H of 3.23, 6.46 and 9.69, respectively. Therefore, it is thus firmly established that the point of maximum heat flux to the lower surface basically coincides with the separation point. For the time being, it is worth taking a closer look at the peak values for the $H = 9.69$ case. Referring to Fig. 5(a), it is clearly noticed a second point of maximum heat transfer coefficient at the vicinity of the step base, more precisely for section $X = 46.8$. This behavior differs from the other two cases, i.e., frontal-face height H of 3.23 and 6.46.

A detailed and careful effort was made in order to identify the physical process responsible for this second peak on the heat transfer coefficient C_h. According to equations (1) and (2), the heat transfer coefficient can be separated into two parts: one part related to the contribution of the incident energy and the other one to the contribution of the reflected energy from the surface of the step. In this fashion, Figs. 6(a-c) demonstrates the distribution of these two contributions along the lower surface for height H of 3.23, 6.46,

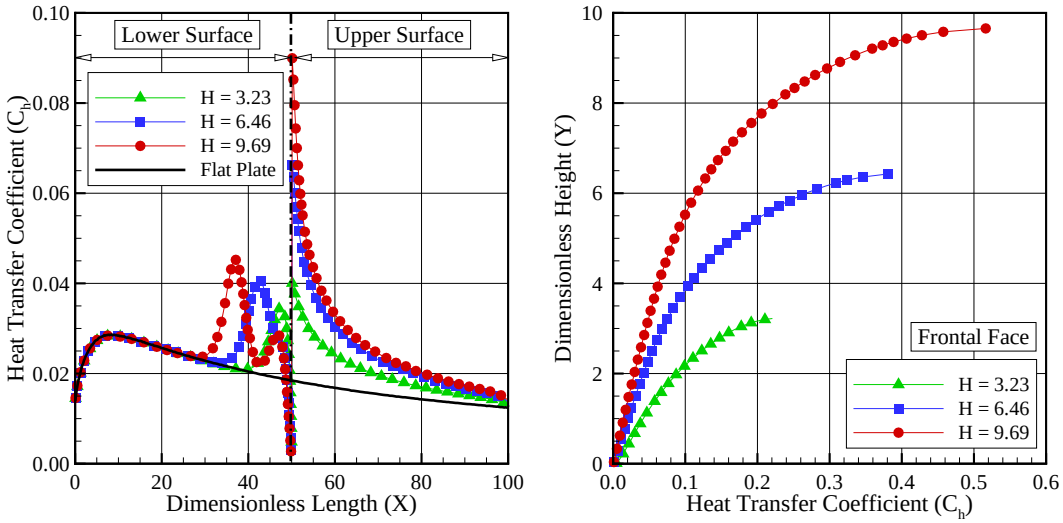

(a) Lower and upper surfaces

(b) Frontal-face surface

Figure 5. Distribution of the heat transfer coefficient C_h along (a) the lower and upper surfaces and along the (b) frontal-face surface as function of the dimensionless frontal-face height H.

and 9.69, respectively. In this set of plots, C_{hi}, C_{hr}, and C_h correspond, respectively, to the incident, reflected and total heat transfer coefficients.

According to Figs. 6(a-c), it is clearly seen that the maximum point in the heat transfer coefficient distribution is directly related to the incident heat flux to the surface of the step. It is also recognized from these plots the presence of one peak value in the incident distribution C_{hi} for the $H = 3.23$ case, and two peak values for the $H = 9.69$ case. For the intermediate case, $H = 6.46$, it is also seen one peak value in the C_{hi} distribution, however, there is sufficient evidence of the formation of a second peak value. It should be remarked that the incident heat flux C_{hi} to the surface is composed by the contributions of the translation, rotation and vibration energies of the molecules, as defined in equation (2). In this sense, Figs. 7(a-c) displays the contributions of each energy mode along the lower surface for the height H of 3.23, 6.46, and 9.69, respectively. In this group of diagrams, the sub-indices T, R, and V refer, respectively, to translation, rotation and vibration energy modes of the molecules.

Referring to Fig. 7, it is firmly established that the three energy modes contribute to the formation of the peak values in the heat transfer distribution to the lower surface. It is seen that the translation energy contributes to the largest portion, followed by the rotation and, finally, by the vibration energy. The physical process, related to the presence of the peak values in the heat transfer coefficient at sections $X =$ 47.5, 42.4, and 37.0, can be explained as follows. As shown earlier, the location of the peaks corresponds to the recirculation zone. Part of the molecules confined in the recirculation zone collides with the frontal-face surface of the step. These molecules exchange energy with the frontal-face surface (see Fig. 5(b)) and reflect from the surface with energy correspondent to the step surface temperature T_w. Back to the recirculation zone, in a clockwise direction (see Fig. 4), part of these molecules collides with the lower surface and exchanges energy with the surface. It is important to emphasize that, although these molecules have a low energy when compared to those from freestream, these molecules contribute significantly to enhance the heat flux to the surfaces due to a large number of molecules in this region, not only colliding with the lower surface but also colliding with the frontal face of the step, as shown in Fig. 3. Nevertheless, it remains an open question the physical process responsible for the second peak in the heat flux to the lower surface for the height $H = 9.69$ case, located at $X = 46.8$. A possible explanation will be given in subsequently sections.

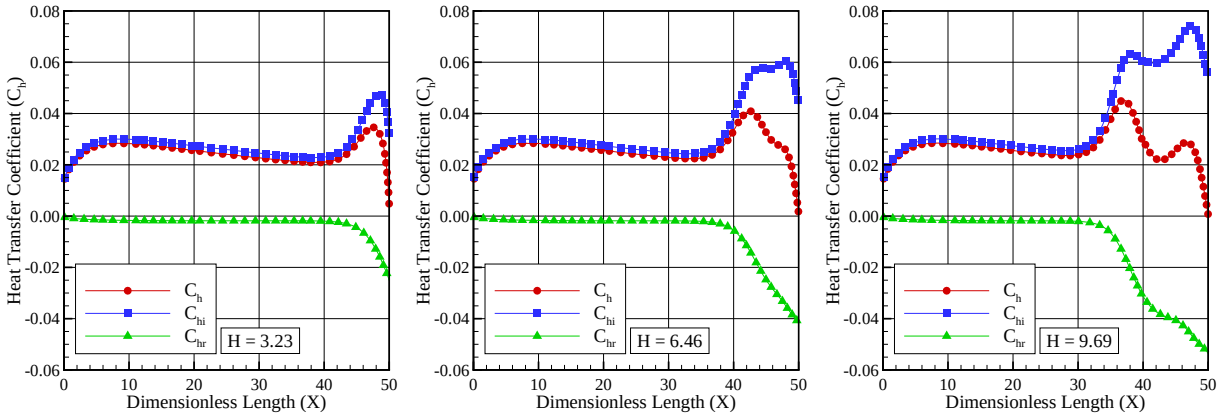

Figure 6. Distribution of incident, reflected and total heat transfer coefficients along the lower surface of the step with height H of (a) 3.23, (b) 6.46, and (c) 9.69.

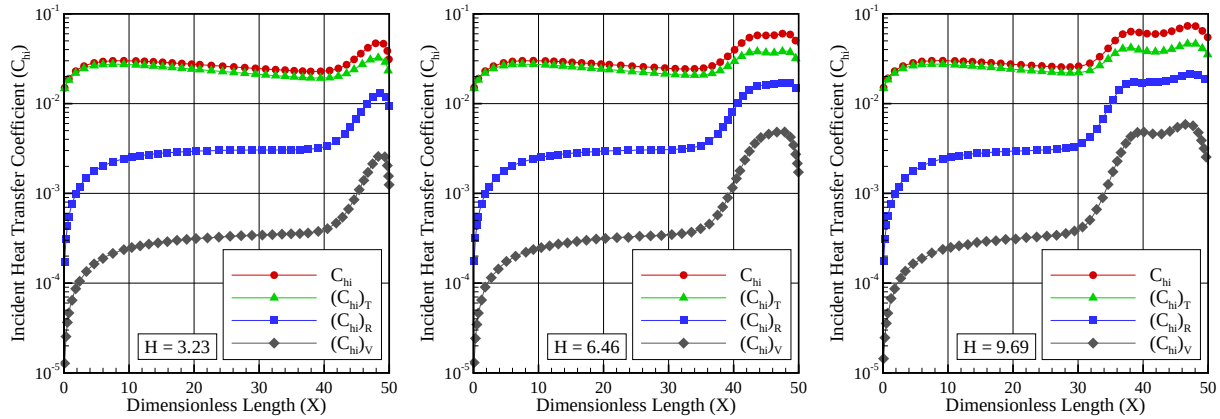

Figure 7. Contribution of translation, rotation and vibration energies modes to the incident heat transfer coefficient along the lower surface of the step with height H of (a) 3.23, (b) 6.46, and (c) 9.69.

C. Pressure Coefficient

The pressure coefficient C_p is defined as follows,

$$C_p = \frac{p_w - p_\infty}{\frac{1}{2}\rho_\infty U_\infty^2} \tag{3}$$

where the pressure p_w on the body surface is calculated by the sum of the normal momentum fluxes of both incident and reflected molecules at each time step as follows,

$$p_w = p_i - p_r = \frac{F_N}{A\Delta t}\sum_{j=1}^{N}\{[(mv)_j]_i - [(mv)_j]_r\} \tag{4}$$

where v is the velocity component of the molecule j in the surface normal direction.

The impact on the pressure coefficient C_p caused by changes in the frontal-face height h is depicted in Figs. 8(a,b) for lower, frontal face, and upper surfaces. According to this group of plots, it is noted that

the pressure coefficient behavior follows the same trend as that shown for the number flux in the sense that: (1) the pressure coefficient behavior along the step surface is similar to that for the flat-plate case at the vicinity of the sharp leading edge, (2) the upstream disturbances in the pressure coefficient C_p, due to the presence of the step, were felt up to section X corresponding to approximately 32.6, 38.1, and 43.4 for steps with height H of 9.69, 6.46, and 3.23, respectively, (3) from these sections up to the step position, $X = 50$, the pressure coefficient C_p increases dramatically when compared to that for the flat-plate case, (4) the maximum values for the pressure coefficient C_p along the the lower surface occur at the stagnation point, at the lower-surface/frontal-face junction, (5) along the frontal-face surface, the peak value for C_p occurs close the frontal-face/upper-surface junction, similar to that peak value location for the heat transfer coefficient.

For comparison purpose, the maximum values for C_p on the frontal face are around 0.64, 1.17 and 1.68 for height H of 3.23, 6,46 and 9.69, respectively. In contrast, the maximum value of C_p for the flat-plate case, i.e., a flat plate without steps, is around 0.0393 at section $X = 25.96$ in the lower surface. Therefore, C_p of 0.64, 1.17 and 1.68 correspond respectively to 16.28, 29.77 and 42.75 times the pick value for the flat-plate case, which corresponds to a smooth surface.

It is noteworthy that, similar to the number flux, the pressure coefficient rise at the vicinity of the frontal face is directly related to the recirculation zone that forms ahead of the step. This pressure rise is explained by the fact that molecules, confined in the recirculation zone, collide with the lower surface and with the frontal face of the step, causing an increase in the normal momentum to both surfaces of the step.

The behavior for the distribution of wall pressure p_w along the lower surface for the $H = 3.23$ case can be qualitatively compared to that presented by Pullin and Harvey.[7] Pullin and Harvey[7] have numerically investigated a rarefied hypersonic flow over a forward-facing step by employing the DSMC method. For the flow conditions, they assumed N_2 as the working fluid, freestream Mach number M_∞ of 22.9, and freestream temperature T_∞ of 20 K. The forward-facing step, located at $48\lambda_\infty$ downstream of the flat-plate leading edge, was kept to a wall temperature T_w of 288 K, which corresponded to $T_w/T_\infty = 14.4$. Although it was not directly defined in the technical note, the frontal-face height h is in the range of $3\lambda_\infty < h < 5\lambda_\infty$. According to the authors, the flow and body conditions were chosen in order to reproduce the experiments conducted by Jeffrey (1973), a private communication cited by Pullin and Harvey.[7]

In this scenario, Fig. 9 displays the pressure ratio p_w/p_∞ for the $H = 3.23$ case investigated in the present account and those numerically investigated by Pullin and Harvey[7] and experimentally by Jeffrey (1973). In this set of diagrams, X' and Y are, respectively, the horizontal length $(x - L)$ and the vertical length y

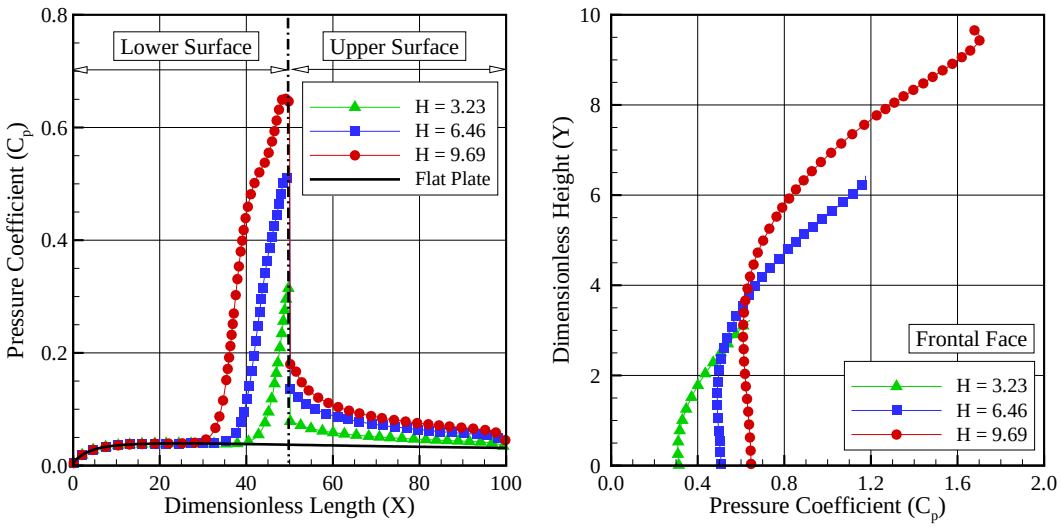

(a) Upper and lower surfaces

(b) Frontal-face surface

Figure 8. Distribution of the pressure coefficient C_p along (a) the lower and upper surfaces and along the (b) frontal-face surface as function of the dimensionless frontal-face height H.

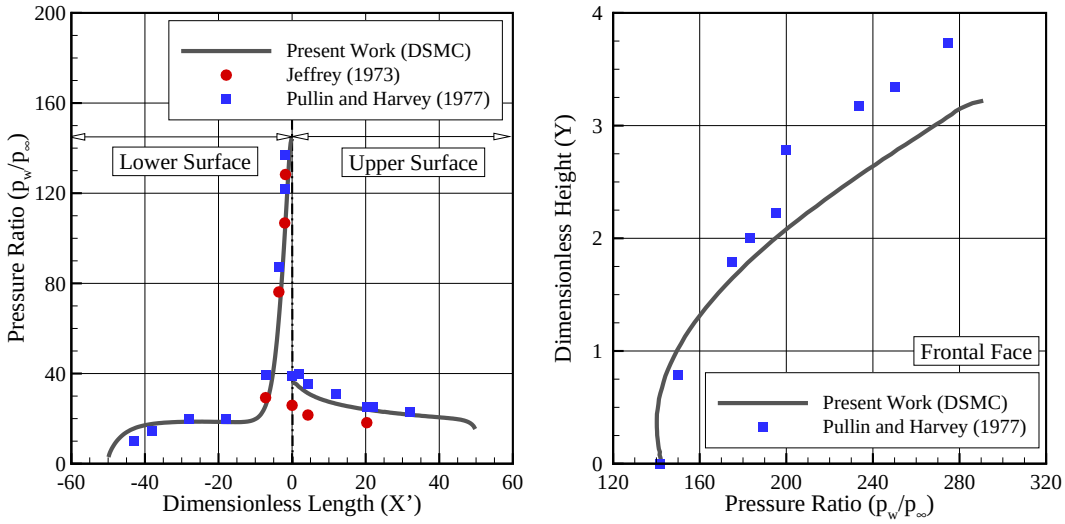

(a) Upper and lower surfaces

(b) Frontal-face surface

Figure 9. Comparison of pressure ratio (p_w/p_∞) distribution acting along the (a) lower and upper surfaces, and (b) along the frontal-face surface for the $H = 3.23$ case.

Table 4. Comparison of freestream and flow conditions for the present DSMC simulation and for that presented by Pullin and Harvey.[7]

Work	Gas	M_∞	T_∞(K)	T_w(K)	T_w/T_∞	h/λ_∞
Pullin and Harvey[7]	N_2	22.9	20.00	228	14.4	3 to 5
Present DSMC work	O_2,N_2	25.0	219.69	880	4.0	3.23

normalized by the mean free path λ_∞. According to Fig. 9, the comparison presents a good qualitative agreement on the pressure ratio distribution along the lower, frontal face, and upper surfaces of the step. Despite of some differences in terms of the flow conditions, summarized in Tab. 4, the comparison seems to be relevant in the sense that the pressure ratio p_w/p_∞ demonstrates a similar trend for the three investigations.

D. Skin Friction Coefficient

The skin friction coefficient C_f is defined as follows,

$$C_f = \frac{\tau_w}{\frac{1}{2}\rho_\infty U_\infty^2} \tag{5}$$

where the shear stress τ_w on the body surface is calculated by the sum of the tangential momentum fluxes of both incident and reflected molecules impinging on the surface at each time step by the following expression,

$$\tau_w = \tau_i - \tau_r = \frac{F_N}{A\Delta t}\sum_{j=1}^{N}\{[(mu)_j]_i - [(mu)_j]_r\} \tag{6}$$

where u is the velocity component of the molecule j in the surface tangential direction.

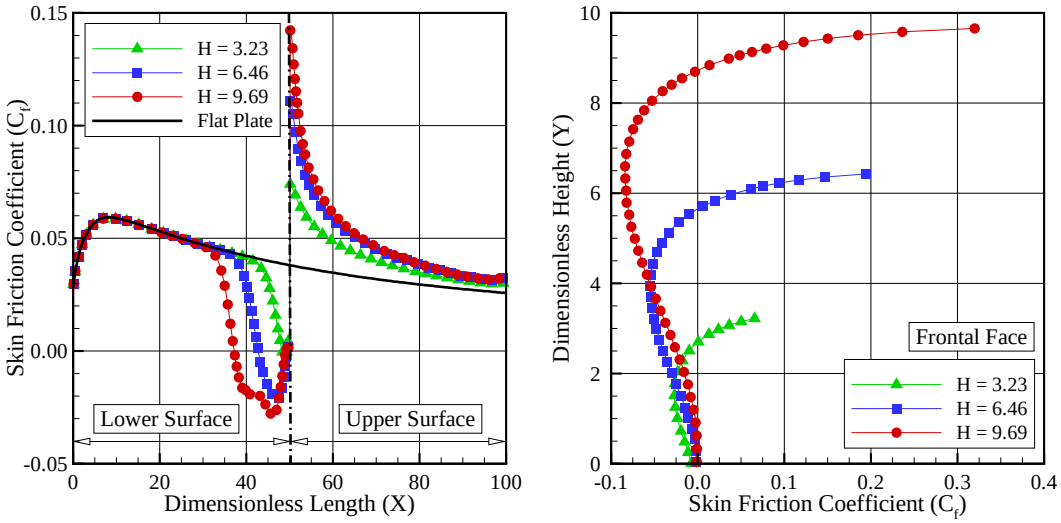

(a) Upper and lower surfaces

(b) Frontal-face surface

Figure 10. Distribution of the skin friction coefficient C_f along (a) the lower and upper surfaces and along the (b) frontal-face surface as function of the dimensionless frontal-face height H.

It is worthwhile to note that for the special case of diffuse reflection, the gas-surface interaction model adopted herein, the reflected molecules have a tangential moment equal to zero, since the molecules essentially lose, on average, their tangential velocity components. In this fashion, the tangential momentum flux of the incident molecules is defined as follows,

$$\tau_w = \tau_i = \frac{F_N}{A\Delta t}\sum_{j=1}^{N}\{[(mu)_j]_i\} \tag{7}$$

The distribution of skin friction coefficient C_f along the step surfaces – lower, frontal face, and upper – is displayed in Fig. 10 as a function of the step height h. Once again, in this set of plots, X and Y represent, respectively, the lengths x and y normalized by the freestream mean free path λ_∞.

Looking first to Fig. 10(a), it is observed that the upstream disturbances, due to the presence of the steps, are felt in the skin friction coefficient C_f approximately up to section X of 32.6, 38.1, and 43.4, for height H of 9.69, 6.46, and 3.23, respectively. From this position up to the step position, $X = 50$, the skin friction coefficient C_f decreases, when compared to that for the flat-plate case, and reaches zero for section X of 37.3, 42.8, and 48.3 for height H of 9.69, 6.46, and 3.23, respectively. After that, as a result of the recirculation region, the skin friction coefficient C_f continues to decrease up to a minimum point. After the minimum point, C_f increases again and reaches values close to zero at the stagnation point at the base of the step. Along the upper surface, the skin friction coefficient C_f presents the maximum value at the step shoulder,then drops off downstream and reaches the value observed for the flat-plate case.

Turning to Fig. 10(b), along the frontal face, the skin friction coefficient C_f is basically zero at the step base. After that, it is negative from the step base up to the flow reattachment point. From this point up to the step corner, the skin friction coefficient drastically increases, since this is basically a region exposed to a high speed flow. Afterwards, due to the flow expansion around the step corner, the skin friction coefficient C_f diminishes by approximately 50% in comparison to the values observed at the beginning of the upper surface. It should be mentioned that the section corresponding to the condition of $C_f = 0$ ($\tau_w = 0$) was used to define the separation point.

A more careful analysis in the distribution of the skin friction coefficient C_f reveals important flow peculiarities at the vicinity of the step base. As shown in Fig. 10(a), the skin friction coefficient C_f, after

reaching the minimum negative value, it increases again and reaches values around zero at the stagnation point. A magnified view of the stagnation region indicates that the skin friction coefficient C_f becomes positive in this region, more precisely at section X of 49.3, 49.4, and 49.1 for height H of 3.23, 6.46, and 9.69, respectively, as illustrated in Fig. 11.

Therefore, the skin friction coefficient starts with positive values near the sharp leading edge, it becomes negative along the lower surface, then it changes to positive values very close to the stagnation point. It should be emphasized that the change from positive to negative value in the skin friction coefficient C_f indicated a change in the flow direction, and resulted in a recirculation region as shown in Fig. 4. Consequently, similarly, a new signal change, from negative to positive value, indicates a possibility of a second recirculation region very close to the step base. In attempting to assess such effect, a magnified view of Fig. 4 was obtained at the vicinity of the step base. It is clearly noticed the formation of a second recirculation region in a much smaller scale than that one shown previously in Fig. 4.

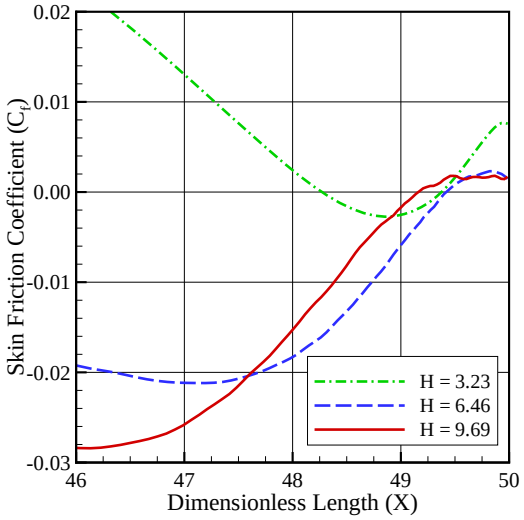

Figure 11. Distribution of skin friction coefficient C_f at the vicinity of the frontal face as a function of the dimensionless frontal-face height H.

For completeness, Fig. 12 demonstrates this second recirculation zone very close to the step base. In this group of plots, Y_h represents the vertical distance y normalized by the frontal-face height h, and X'_h refers to the horizontal distance $(x - L)$ also normalized by height h. From this set of plots it is very encouraging to observe that, for the conditions investigated in this work, a second recirculation region appears between the first recirculation region and the step base.

This second recirculation zone is a very small region for the $H = 3.23$ case, it increases for the $H = 6.46$ case, and it becomes a well defined region for the $H = 9.69$ case. Of particular interest is the flow direction

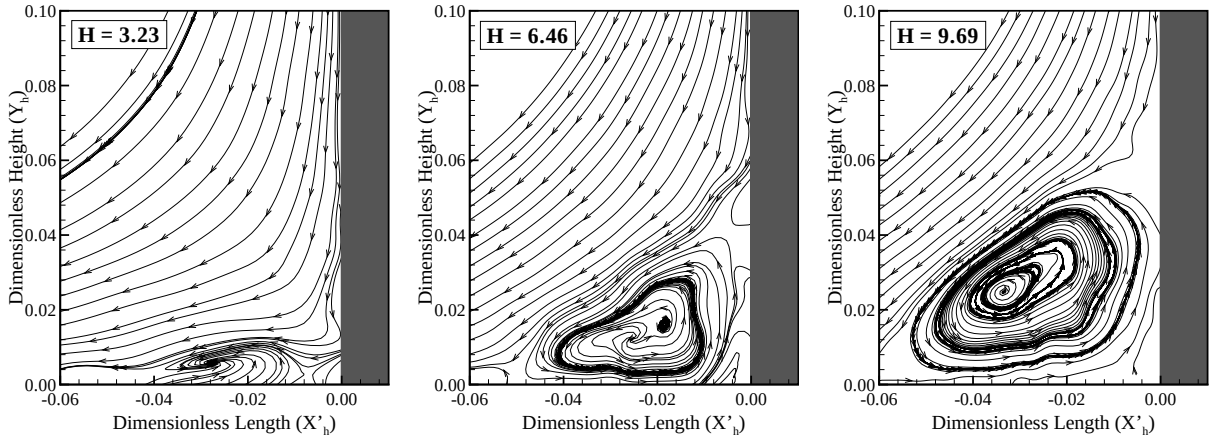

Figure 12. Distribution of the streamline traces at the vicinity of the step base for dimensionless frontal-face height H of (a) 3.23, (b) 6.46, and (c) 9.69.

in both recirculation regions. The flow in the first recirculation regions turns in the clockwise direction, whereas the flow in the second recirculation region turns in the counterclockwise direction. Also, it should be emphasized that the second recirculation region is formed by molecules with low velocity. On the other hand, it is a region with a high concentration of molecules. As a base of comparison, the local density ρ is from 30 times (for $H = 3.23$ case) to 70 times (for $H = 9.69$ case) larger than the freestream density ρ_∞, as shown by Leite.[20] Confined in this region, part of these molecules collides with the lower surface exchanging energy and linear momentum. Back to the recirculation region, these molecules collides with the step frontal face, exchanging again energy and linear momentum. As a result, a large flux of molecules to both walls is observed at the vicinity of the step base, as indicated in Fig. 3. Consequently, it may be inferred that the behavior of these molecules, confined in this second recirculation region, seems to be responsible for the presence of the second peak on the heat transfer coefficient C_h for the $H = 9.69$ case.

VII. Concluding Remarks

Computations of a rarefied hypersonic flow over forward-facing steps have been performed by using the Direct Simulation Monte Carlo (DSMC) method. The simulations provided information concerning the nature of the aerodynamic properties acting on the surface of the steps. Effects of the frontal-face height on the number flux, heat transfer, pressure and skin friction coefficients for a representative range of parameters were investigated. The frontal-face height ranged from 3 to 9 mm, which corresponded to Knudsen numbers in the transitional flow regime.

The analysis showed that hypersonic flow past a forward-facing step is characterized by a strong compression ahead of the frontal face, which influences the aerodynamics surface properties upstream the frontal face. It was found that the upstream disturbance due to the presence of the steps increased with the frontal-face-height rise. Also, locally high heating rates were observed on the surface upstream the step. The simulations showed that these high heating rates are a consequence of the molecules confined in the recirculation zones.

VIII. Acknowledgments

The authors would like to acknowledge the financial support provided by CNPq (Conselho Nacional de Desenvovimento Cientifico e Tecnologico) under Grant No. 473267/2008-0.

References

[1]Bertram, M. H., and Wiggs, M. M., "Effect of Surface Distortions on the Heat Transfer to a Wing at Hypersonic Speeds", *AIAA Journal*, Vol. 1, No. 6, 1963, pp. 1313–1319.

[2]Hahn M., "Experimental Investigation of Separated Flow over a Cavity at Hypersonic Speed", *AIAA Journal*, Vol. 7, No. 6, 1969, pp. 1092–1098.

[3]Nestler, D. E., Saydah, A. R., and Auxer, W. L., "Heat Transfer to Steps and Cavities in Hypersonic Turbulent Flow", *AIAA Journal*, Vol. 7, No. 7, 1969, pp. 1368–1370.

[4]Grotowsky, M. G., and Ballmann J., "Numerical Investigation of Hypersonic Step-Flows", *Shock Waves*, Vol. 10, 2000, pp. 57–72.

[5]Chapmann, D. R., Kuehn, D. M. and Larson, H. K., "Investigation of Separeted Flows in Supersonic and Subsonic Streams with Emphasis on the Effect of Transition", NACA Report 1356, 1958.

[6]Rogers, E. W. E., Berry, C. J., "Research at the NPL on the Influence at Supersonic Speeds and Low Reynolds Numbers of Thick Laminar Boundary Layers", In Leeuw, J. H., ed., *Advances in Applied Mechanics: Rarefied Gas Dynamics*, Vol. I, Suppl. 3, Academic Press, New York, pp. 574–591, 1965.

[7]Pullin, D. I., and Harvey, J. K., "Direct Simulation Calculations of the Rarefied Flow Past a Forward-Facing Step", *AIAA Journal*, Vol. 15, No. 1, 1977, pp. 124–126.

[8]Stüer, H., Gyr, A., and Kinzelbach, W., "Laminar Separation on a Forward Facing Step", *Eur. J. Mech. B/Fluids*, Vol. 18, 1999, pp. 675–6920.

[9]Camussi, R., Felli, M., Pereira, F., Aloisio, G., and Di Marco, A., "Statistical Properties of Wall Pressure Fluctuations over a Forward-Facing Step", *Physics of Fluids*, Vol. 20, 2008, pp. 075113.

[10]Bogdonoff, S. M. and Kepler, C. E., "Separation of a Supersonic Turbulent Boundary Layer", *Journal of The Aeronautical Science*, Vol. 22, 1955, pp. 414–430.

[11]Bird, G. A.,*Molecular Gas Dynamics and the Direct Simulation of Gas Flows*, Oxford University Press, Oxford, England, UK, 1994.

[12]Bird, G. A., "Monte Carlo Simulation in an Engineering Context," in *Progress in Astronautics and Aeronautics: Rarefied gas Dynamics*, edited by Sam S. Fisher, Vol. 74, part I, AIAA New York, 1981, pp. 239–255.

[13]Bird, G. A., "Perception of Numerical Method in Rarefied Gasdynamics", in *Rarefied gas Dynamics: Theoretical and*

Computational Techniques, edited by E. P. Muntz, and D. P. Weaver and D. H. Capbell, Vol. 118, Progress in Astronautics and Aeronautics, AIAA, New York, 1989, pp. 374–395.

[14]Borgnakke, C. and Larsen, P. S., "Statistical Collision Model for Monte Carlo Simulation of Polyatomic Gas Mixture," *Journal of computational Physics*, Vol. 18, No. 4, 1975, pp. 405–420.

[15]Guo, K. and Liaw, G.-S., "A Review: Boundary Conditions for the DSMC Method," in *35th AIAA Thermophysics Conference*, AIAA Paper 2001–2953, Anaheim, CA, 2001.

[16]Alexander, F. J., Garcia, A. L., and, Alder, B. J., "Cell Size Dependence of Transport Coefficient in Stochastic Particle Algorithms," *Physics of Fluids*, Vol. 10, No. 6, 1998, pp. 1540–1542.

[17]Alexander, F. J., Garcia, A. L., and, Alder, B. J., "Erratum: Cell Size Dependence of Transport Coefficient is Stochastic Particle Algorithms," *Physics of Fluids*, Vol. 12, No. 3, 2000, pp. 731–731.

[18]Garcia, A. L., and, Wagner, W., "Time Step Truncation Error in Direct Simulation Monte Carlo", *Physics of Fluids*, Vol. 12, No. 10, 2000, pp. 2621–2633.

[19]Hadjiconstantinou, N. G., "Analysis of Discretization in the Direct Simulation Monte Carlo", *Physics of Fluids*, Vol. 12, No. 10, 2000, pp. 2634–2638

[20]Leite, P. H. M., *Direct Simulation of the Step Influence on a Reentry Vehicle Surface* (in Portuguese), MS Thesis, INPE, 2009.